# Ultra-short laser pulses propagation through mouse head tissues: experimental and computational study

Diana Galiakhmetova, Viktor Dremin, Aleksandr Koviarov, Dmitrii Stoliarov, Neville Ngum, Raghavan Chinnambedu Murugesan, Rheinallt Parri, Sergei Sokolovski, and Edik Rafailov *Senior Member, IEEE*

***Abstract*—We present a prototype and verification of a multi-channel laser system applicable to optogenetic research. *In vivo* photostimulation of neural cells expressing photoconvertible phytochromes or opsins requires enough light irradiation delivery to the brain that cannot be supported by continues-wave (CW) light sources. The use of ultra-short pulsed (USP) lasers operating in the second near-infrared region (II-NIR) and allowing nonlinear activation and deactivation of the photoactuators is a promising method that allows to increase the penetration depth and provide spatio-temporal localisation of radiation in tissues. This study aimed to investigate the efficiency of USP light propagation in the skin, skull, and brain of the mouse head, as well as to compare it with the corresponding CW radiation propagation in the 750–830 nm and 1086–1183 nm wavelength ranges. The experimental results and computer modelling demonstrate that about 10–12% of the initial laser radiation can reach the brain tissues. These results prove that under certain conditions, the USP laser radiation can reach a penetration depth with required power that will be sufficient for non-linear activation of opsins/phytochromes in the brain of living animals.**

***Index Terms*—ultra-short pulsed laser light; mouse head; light propagation; optical properties; penetration depth; transmittance, fluence rate, optogenetics**

## I. Introduction

OPTOGENETICS is a neuromodulation approach that provides an opportunity to monitor and control the activity of neural cells in areas of the brain where opsins or phytochromes are expressed [1]. Neuronal cells that express light-activating ion channels (opsins) or long-lasting signal transducers (phytochromes) can be easily manipulated with light [2], [3]. Opsins and phytochromes are highly accustomed photoactuators that can easily be switched from resting to signalling state by light illumination [4]–[8]. Since a wide variety of opsins and phytochromes have been discovered and genetically engineered, the absorption spectra of phytochromes cover the wavelength range of 0.5–0.8 $\mu$m [6], while the absorption spectra of opsins are found in almost the entire spectrum of visible light [7], [8]. Under light illumination, opsins expressed in neural cells, cause de- or hyperpolarization of neuron membrane which leads to electrical response within the network in a fraction of a second [9]. In the case of phytochromes, the cell response can be reversed by continues wave (CW) light red and far-red irradiation [5], [6], [10]. These light-sensitive proteins could potentially be used as tools for the adjustment of long-term activity of neuronal cells in brain circuits [11]. Opsins and phytochromes could possibly be applied in the treatment of sensorineural hearing loss [12], [13], mood disorders [14], drug addiction [15], obsessive compulsive disorders [16], inherited retinal [17] and Parkinson's [18], [19] diseases.

Nevertheless, the main hurdle of non-invasive treatment is the delivery of sufficient power for photoconversion after light passing through the skin, skull, and brain [20], [21]. These biological tissues significantly absorb visible light, which can lead to their heating and damage [22]. This effect can be mitigated if the exciting laser operates in the region of the tissue transparency windows instead of the visible spectrum [23]–[25]. L. Shi et al. [23] introduced optical windows of brain tissues in near-infrared regions (NIR). They performed theoretical and experimental studies of the transmission in 50-200 $\mu$m rat brain slices in four NIR transparency windows: (I) ~650–950 nm, (II) ~1100–1350 nm, (III) ~1600–1870 nm, and (IV) ~2100–2300 nm. According to experimental results, the average attenuation lengths of brain tissues in windows I, II, III, and IV are 192.4 $\mu$m, 259.4 $\mu$m, 289.7 $\mu$m, and 248.1 $\mu$m, respectively. The II and III NIR windows have higher attenuation lengths in comparison with visible and I-NIR window regions because the light scattering and absorption decrease according to the Rayleigh and Mie scattering theories. S. Golovynskyi et al. [25] demonstrated that the radiation in one of the transparency windows penetrates both into the brain tissue and into the skin and skull at least two times deeper than visible light. They measured light transmission and absorption of head tissues of healthy 4-month-old male rats and determined the values of attenuation coefficient and attenuation length. The highest light permeability through 1 mm skin, 0.9 mm cranial bone, and 1 mm brain cortex samples in the II-NIR and III-NIR regions. In the II-NIR window, the maximum attenuation length for the skin, bone, and brain cortex samples were 0.44 mm, 0.22 mm, and 1.35 mm, while, in visible range, the values were only 0.36 mm, 0.18 mm, and 0.7 mm, respectively. Since II-NIR lasers can reach deeper layers of head tissues than lasers

This work has been supported by the European Union's Horizon 2020 research and innovation programme under grant agreement No.863214 – NEUROPA project. D.G. gratefully acknowledges funding by the Return to Research grant, Rank Prize. Authors thank Alex Rozhin for providing support in spectrophotometry measurements. (*Corresponding author: Viktor Dremin and Diana Galiakhmetova*)

D. Galiakhmetova, V. Dremin, A. Koviarov, D. Stoliarov, R. Chinnambedu Murugesan, S. Sokolovski and E. Rafailov are with the College of Engineering and Physical Sciences, Aston University, Birmingham, UK (e-mail: d.galiakhmetova@aston.ac.uk, v.dremin1@aston.ac.uk, a.koviarov@aston.ac.uk, d.stoliarov@aston.ac.uk, r.chinnambedu-murugesan@aston.ac.uk, s.sokolovsky@aston.ac.uk, e.rafailov@aston.ac.uk).

N. Ngum and R. Parri are with the College of Health and Life Sciences, Aston University, Birmingham, UK (e-mail: n.ngum@aston.ac.uk, h.r.parri@aston.ac.uk).

operating in the visible spectrum, their use can significantly improve non-invasive neuronal stimulation.

The use of II-NIR lasers in optogenetics has been made possible by recent research demonstrating the nonlinear photoconversion of photoactuators [26]–[29]. S. Sokolovski et al. [29] first predicted and experimentally proved the non-linear photoconversion of *Deinococcus deserti* bacteriophytochrome (*Dd*BPhy) that was irradiated by a tunable pulsed laser operating at wavelengths of 1.1-1.3 $\mu$m. Two-photon absorption can also switch opsins into the active state in this wavelength range.. For example, modified proton-pumping rhodopsins from Gloeobacter violaceus (GRr3) have a linear activating wavelength around 619 nm [7], while cyanorhodopsins (CyR) have the maximum absorption peak at wavelength of 550 nm [30]. This may allow the actuation of opsins and phytochromes by two-photon absorption in the wavelength range of 1.1–1.3 $\mu$m [29], which is covered by the II-NIR transparency window [23]–[25].

However, the *in vivo* use of II-NIR lasers for optogenetics requires a detailed study of the tissue interaction with ultrashort pulses (USP), since two-photon conversion of photoactuators is possible only at high peak power [29].

In the literature, the optical properties of head tissues are mainly studied with the use of CW lasers [23], [25], [31]–[35]. However, the experimental results of attenuation length values vary significantly in studies of different research groups. The attenuation length of brain tissues can be in the range of 0.24–1.54 mm depending on the measurement methods, the age of rats, and the wavelength of a light source. For skin tissues, the experimental results of the light propagation are also different. C. Sabino et al. [33] investigated the light interaction with the skin of 4–6 week-old healthy mice. Skin samples included the epidermis, dermis, and adipose tissue. The measured attenuation length was up to 3.5 mm, which is 7 times higher than the experimental values obtained by S. Golovynskyi et al. [25] and M. Ozturk et al. [34]. Here, the attenuation length values for skin can also depend significantly on the age of the animals, sample storage conditions, and measurement approach used. The inconsistent experimental results presented in the literature require additional research to apply II-NIR lasers for optogenetics.

For the USP lasers, several independent studies demonstrated that pulsed light allows a more efficient transfer of energy and can generate less tissue heating compared with CW light [36]–[41]. A. Barbora et al. [38] experimentally proved that high-frequency pulsed wave irradiation penetrates deeper than low-frequency pulsed and CW irradiations. They used lasers of various modes operating at a wavelength of 808 nm (CW laser: 165 mW; pused lasers: 50 fs, 500 Hz, 2.55 W and 5 fs, 71.4 MHz, 216 mW). For chicken breast samples, the penetration depths were 1.13 ± 0.21 mm, 3.24 ± 0.48 mm, and 3.56 ± 0.34 mm for CW, low-frequency, and high-frequency pulsed lasers, respectively. However, there was a high measurement uncertainty and a small difference between the depth values for pulsed lasers. On the other hand, T. Ando et al. [42] demonstrated that the transmittance of laser power through mouse scalp and skull does not differ significantly on laser pulse frequency. In the experiments, they used 810 nm CW laser, 10 Hz and 100 Hz pulsed lasers and did not observe a difference in transmitted power. Although this result can be explained by the fact that mouse head samples are quite thin and the optical properties do not differ significantly when CW or microsecond pulsed lasers are used. According to B. Shariati B. K. et al. [43] study, only if the pulse width is shorter than 100 ps, the absorption and scattering coefficients significantly drop with the reduction of the pulse duration. This effect is observed due to the increase in the frequency distribution width of the pulse and the decrease in the interaction of the pulse with the skin. However, whether it will be observed at longer wavelengths (>850 nm) and whether the experimental data of the head tissues will agree with the computational model remains unexplored. Thus, the optical properties of biological tissues with the use of USP lasers are shown in [38]–[45], but the interaction of head tissues with a USP laser applicable for two-photon optogenetics with required wavelength and peak power has not yet been studied.

We have developed a tunable laser that can be a prototype of laser technology applicable for optogenetic therapy. In this paper, we investigate the light-tissue interaction by using a tunable USP laser operating in the first two biological windows. These wavelength ranges were chosen to cover linear absorption spectra for phytochrome deactivation (750–830 nm) [6], [10], [29] and two-photon absorption spectra for phytochrome [29] and opsin [8], [30] activation (1.1–1.2 $\mu$m). The research aims to assess the attenuation of light into brain tissue, taking into account the absorption and scattering of the skin, skull, and upper layers of the brain. We present the results of the laser light transmittance through *ex vivo* samples of the adolescent mouse head. The study is also supported by spectrophotometric measurements and numerical modelling of light propagation in mouse head samples.

## II. Material and Methods

### A. Sample preparation

All experiments were approved by local ethical review and performed in accordance with the UK Animals Scientific Procedures Act of 1986 and current EU legislation. Experiments were planned taking into account 3Rs, replacement, refinement, and reduction. Fresh samples of skin, skull, and brain tissues were taken from wild type mice of C57BL/6J genetic background [46], kept on ice and used in the same day in all experiments. Samples were obtained from two healthy male adolescent mice (postnatal P43) using the standard protocol. Mice were humanely killed by isoflurane overdose followed by cervical dislocation. Heads were shaved to remove fur from the skin-covered frontal and parietal bones. Small incisions were made to cut a 15×15 mm square sample of the head skin. The total thickness of this tissue was 0.5 mm. Fig. 1 shows a schematic illustration of mouse head tissues.

Before placing the skin sample between the cover glass slides, two 0.5 mm thick restrictors were glued to the upper and lower parts of the coated glass to avoid deformation of the skin and brain sample. For the undamaged extraction of the mouse brain, the cranial bone was dissected at the site of the interfrontal and mendosal sutures. The part containing

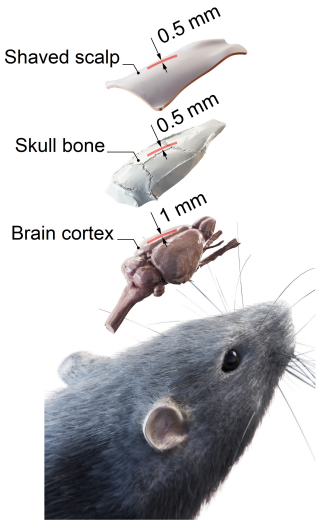


Fig. 1: Dimensions of the mouse head tissues samples prepared for laser irradiation transmission measurements: shaved skin, skull, and brain slice with thicknesses of 0.5 mm, 0.5 mm, and 1 mm, respectively.

frontal, parietal, and interparietal bones was used for optical measurements. Parietal bone thickness ranged from 0.48 to 0.52 mm for different mouse samples. The thickness of the skull bone was determined with a digital micrometer with a resolution of 0.001 mm. The brain was cut into three slides from the cortex. The thickness of each sample was 1 mm. To prevent the brain from leaking or drying out, the sample and 1 mm inserts were placed between cover glass slides. Fig. 2a,b shows the brain cortex located between the glasses and the integrating sphere with photodiode detector, which is used to measure the transmission of pulsed laser light.

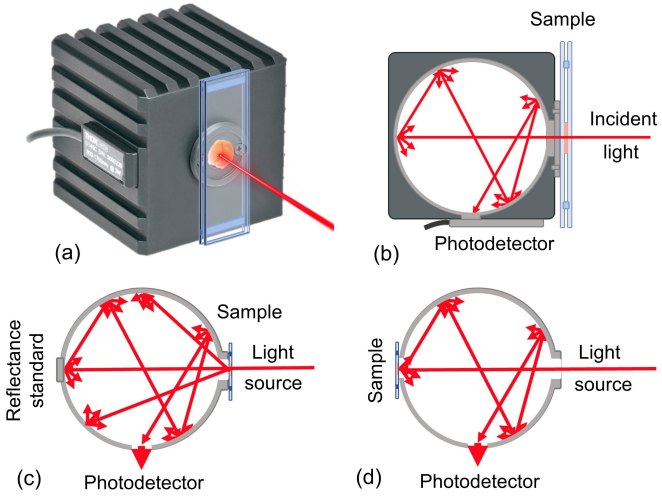


Fig. 2: (a) Principal scheme of the pulsed laser light transmittance measurement; (b) schematic view of the directionality of the transmitted light in an integrating sphere photodiode power sensor. Different operational modes of the spectrophotometer integrating sphere for (c) total transmittance and (d) diffuse reflectance measurements.

### B. Spectrophotometry

First, we investigated the tissue samples using a spectrophotometry technique. The total transmission and diffuse reflectance spectra of mouse head tissues were measured using a spectrophotometer (PerkinElmer LAMBDA 1050+ UV/Vis/NIR spectrophotometer, USA) with 60 mm InGaAs integrating sphere. The sphere has two baffles that shield the sample beam target area from the detector field-of-view. This avoids collecting specularly reflected light from the sample. The measurements were performed in a broad wavelength range of 350–1800 nm. All measurements were made at room temperature (20°C).

For each sample, two types of spectrophotometer configurations were used (Fig. 2c,d). In the first configuration, a sample was located between the integrating sphere and the light source. The additional window in the sphere was closed by a reflectance standard. The transmitted light passing through biological tissue and re-reflected from the walls of the sphere was collected by a photodetector. The second operating mode allows to measure diffuse reflectance spectra of mouse head tissues. A light beam passed unhindered through the first window in the integrating sphere and was then reflected by a sample, which closed the second window.

To process the experimental results and determine the transport coefficients, a combination of the inverse adding–doubling (IAD) method with a corrective Monte Carlo (MC) calculation was used [47]. These methods are widely employed in tissue optics to process the data obtained by integrating sphere-enabled spectrophotometry [48], [49] and used realisation takes into account all the interactions of a sample sandwiched between glass slides. The IAD method allows one to determine the tissue absorption and scattering coefficients using the values of the diffuse reflectance and total transmission coefficients. The anisotropy factor $g$ for brain tissues for the considered wavelength range is between 0.7 and 0.9 [32], [50]. For the IAD calculations, an anisotropy factor of 0.9 was chosen, which most closely characterises the wavelength range in which the experimental system operates.

As the initial values of $\mu_a$ and $\mu_s'$, we used the solutions to the system of the following equations:

$$\frac{\mu_s'}{\mu_a+\mu_s'} = \begin{cases} 1-\left(\dfrac{1-4R_d-T_t}{1-T_t}\right)^2, & \text{if } \dfrac{R_d}{1-T_t} < 0.1 \\ 1-\dfrac{4}{9}\left(\dfrac{1-R_d-T_t}{1-T_t}\right)^2, & \text{if } \dfrac{R_d}{1-T_t} \geq 0.1 \end{cases}, \tag{1}$$

$$(\mu_a+\mu_s')l = \begin{cases} -\dfrac{\ln T_t \ln(0.05)}{\ln R_d}, & \text{if } R_d \leq 0.1 \\ 2^{1+5(R_d+T_t)}, & \text{if } R_d > 0.1 \end{cases}, \tag{2}$$

where $R_d$ is the measured value of diffuse reflectance, $T_t$ is the measured value of total transmission, and $l$ is the thickness of the tissue.

The MC method was used to correct for the light loss at the sample edges, which is not collected by the integrating sphere. The calculated lost light for a given set of optical properties

was taken into account within the subsequent iteration of the calculation using the adding–doubling method. This process was repeated as long as the optical properties were not stable, that is, until the changes in the calculated scattering and absorption values were less than 0.01 $mm^{-1}$ between iterations. As an iterative procedure, the Nelder-Mead simplex method was used [51]. As a criterion for the completion of the iterative procedure, we used the condition:

$$\frac{\mid R_d^{exp} - R_d^{calc} \mid}{R_d^{exp}} + \frac{\mid T_d^{exp} - T_d^{calc} \mid}{T_d^{exp}} < 0.0001, \qquad (3)$$

where $R_d^{exp}$, $R_d^{calc}$, $T_d^{exp}$, and $R_d^{calc}$ are the experimentally determined and theoretically calculated diffuse reflectance and total transmission, respectively.

### C. Tunable ultra-short pulsed laser system

Transmission measurements of mouse head tissues were performed using pulsed and CW lasers operating in the second biological window. For an accurate comparison of the techniques, collimated beams of CW and pulsed lasers were directed to the same spot of sampling material. The experimental setup included three blocks (Fig. 3). The first block was a pulsed laser operating at a wavelength of 750–830 nm (1st range in further text), while two others were 1086–1183 nm (2nd range in further text) CW and pulsed lasers.

Block 1 was designed to measure tissue transmittance in the first tissue transparency window. The 130 fs pulsed titanium-sapphire (Ti:Sa) laser (M squared Sprite XT), tunable in the 750–830 nm wavelength range, was attenuated to 20 mW average power. The repetition rate was 78 MHz. The collimated laser beam with a diameter of 200 $\mu$m was directed by a system of optical lenses. In the experiments, the beam was split by a plane-parallel plate to control the incident and transmitted power. An integrating sphere InGaAs photodiode sensor (Thorlabs S145C) was attached to the measuring sample to detect passing light. A schematic view of the reflection of transmitted light in an integrating sphere photodiode power sensor is shown in Fig. 2a. Block 2 of the experimental setup included a synchronously pumped optical parametric oscillator (OPO). The Ti:Sa laser was tuned to emit a certain wavelength in the range of 750–830 nm which, after passing through the OPO, allowed us to obtain laser radiation with the corresponding wavelength in the range of 1086–1183 nm. The average optical power passed to the sample was 20 mW, while the pulse duration was about 300 fs. The laser beam was collimated and focused into a spot with a diameter of 230 $\mu$m. To compare the transmittance of mouse head tissues irradiated with pulsed and CW lasers, we developed a tunable CW laser operating at a wavelength of 1086–1183 nm. Block 3 is composed of a system of optical lenses and mirrors, a fibre coupled gain chip (Innolume GM-1140-120) and a 1200 lines/mm diffraction grating that allowed us to change the wavelength with a step equivalent to the step value of the pulsed laser in block 2. The optical system was established in such a way that the beam directions and spot sizes were the same for pulsed and CW lasers. The profile and beam diameter were controlled by a laser beam profiling camera.

### D. Fluence rate distribution

To calculate the penetration depth of pulsed radiation into head tissues and the corresponding attenuation, the fluence rate was calculated. We used the diffusion approximation to the radiative transfer equation. The diffusion equation is valid when the scattering is large compared to the absorption and when studying diffuse light propagation, i.e. at sufficient distances from any light source. The analytical solution of the diffusion equation is classic [52]. In this work, we solve the diffusion equation numerically using a COMSOL Multiphysics software solution. The numerical solution is based on the Finite Element Method (FEM), in which the geometry studied is divided into a finite element mesh [53]. One of the main motivations for applying FEM to solve light propagation problems is the ability to use arbitrary geometries.

The diffusion equation is given in Eq. 4:

$$\frac{\partial \Phi(\vec{r},t)}{c' \partial t} + \mu_a \Phi(\vec{r},t) - \nabla \cdot [D \nabla \Phi(\vec{r},t)] = S(\vec{r},t), \qquad (4)$$

where $\Phi$ is the fluence rate; $c'$ is the speed of light in the tissue, as determined by the relative refractive index; $D$ denotes the diffusion coefficient; $\mu_a$ is the absorption coefficient; $S$ describes the light source.

The diffusion coefficient is defined as

$$D = \frac{1}{3(\mu_a + \mu_s')}, \qquad (5)$$

where $\mu_s'$ is the reduced scattering coefficient.

In COMSOL Multiphysics, the Helmholtz representation of Eq. 4 is used. A translation of the diffusion equation can be found in Ref. [54]. The Helmholtz representation of the diffusion equation is given by

$$\nabla(-c\nabla u) + au = f, \qquad (6)$$

where $c = D$, $u = \Phi$, $a = \mu_a$, $f = S$.

A three-layer tissue model (skin, skull bone, and brain tissue) was used to assess the fluence rate. The thicknesses of the layers corresponded to the thicknesses of the experimentally measured samples. The absorption and scattering coefficients of each layer used in the current stage of the study were obtained from the results of spectrophotometric measurements. We have simulated the interaction of pulsed radiation with mouse head tissues in two wavelength ranges that correspond to experimental measurements. The parameters of the laser radiation also coincided with the parameters of the USP laser used.

## III. Results and Discussion

### A. Spectrophotometry

The optical properties of freshly prepared tissue samples (0.5 mm skin, 0.5 mm skull bone, and 1 mm brain) were measured using UV/Vis/NIR spectrophotometer. Fig. 4 shows transmittance and diffuse reflectance spectra with three tissue transparency windows separated by oxy- and deoxyhemoglobin absorbance (∼400–700 nm) and water absorption peaks (∼1450 nm, ∼1950 nm). Transmittance spectra clearly

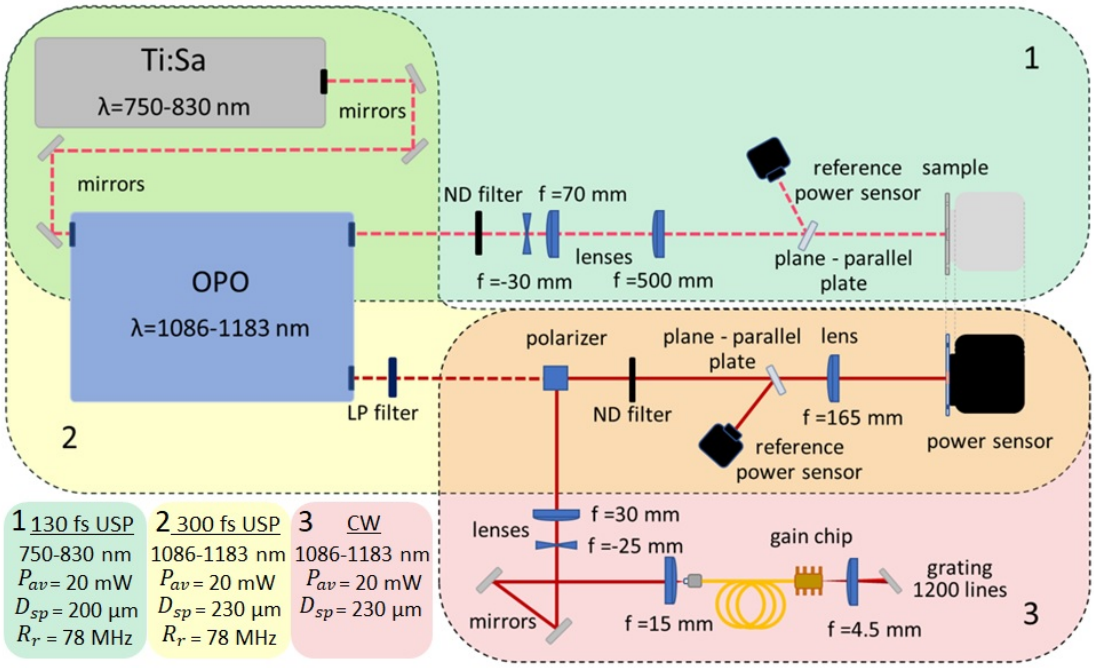


Fig. 3: Flowchart of the developed experimental setup to measure the light transmittance through mouse head tissues. Block 1: a sample was irradiated with a pulsed laser operating at a wavelength of 750–830 nm. Block 2: the tissue samples irradiated with pulsed laser operating at 1086–1183 nm wavelength range. Block 3: the tissue samples irradiated with CW laser (1086–1183 nm) at the same point as pulsed laser in the block 2.

demonstrate three biological windows in the NIR region (Fig. 4a). The first (I) one covers a wavelength region of ∼700–970 nm, while the second (II) and third (III) windows can be identified in ∼1000–1350 nm, ∼1550–1870 nm, respectively.

The skull bone demonstrated the highest transmission in the wavelength range of 890–910 nm (95%). However, the difference between the highest transmission values of skull tissue in the first and second windows does not exceed 3% (Fig. 4a). For both the skin and brain samples, the maximum transmittance is in the second tissue transparency window. The highest transmission for skin is 62%, while for brain it is 47%. In this region, all spectra have a conspicuous region at the wavelength of around 1195 nm that is characterised by the light absorption of water [55]. In addition to this region, water absorption can be observed at wavelengths of ∼975 nm and ∼1450 nm. Absorption by tissue proteins results in slight deviations of the spectra in the wavelength regions of 805–1100 nm and 1420–1540 nm. The third NIR region demonstrates the lowest transmittance for all biotissue samples (Fig. 4b). This ratio can depend on the specific type of tissue samples, animal age and the sample preparation method.

The irradiation transport coefficients of the tissue were calculated from the transmission and diffuse reflectance values obtained experimentally. Therefore, using IAD method-based modelling, the absorption and scattering coefficient spectra were reconstructed (see Fig. 5).

In the absorption coefficient spectra (Fig. 5a), the absorption bands of blood deoxyhemoglobin (∼420 and ∼550 nm) and water (∼1450 nm) mostly dominate the spectral range. The absorption bands of water at ∼975 and ∼1195 nm were considerably lower. The scattering spectra of the tissue samples gradually decreased towards longer wavelengths, which were generally consistent with the character of the spectral behaviour of the scattering coefficient of biotissue samples. Fig. 5b shows approximations of the wavelength dependence of the reduced scattering coefficient by simple power functions.

The main transmittance regions in the spectra are associated with absorption of blood, water, collagen, other proteins and lipids depending what tissues samples were examined. In the second NIR region, the influence of these components on tissue transmittance is significantly lower. It is quite important to note that there is a significant decrease in scattering in this area. Therefore, the advantages of using the second biological window compared to the first one, are undoubted. Lasers operating at 1.1–1.35 $\mu$m wavelength can potentially be used for non-linear conversion because of less absorption in this wavelength region.

Furthermore, we evaluated the penetration depth of radiation into head tissues ($\delta$). The evaluation of penetration depth, defined as the depth for which the intensity of a light beam is attenuated 2.7 times, was performed using the following equation:

$$\delta = \frac{1}{\sqrt{3\mu_a(\mu_a + \mu_s')}}. \tag{7}$$

The result of the calculated tissue penetration depth is

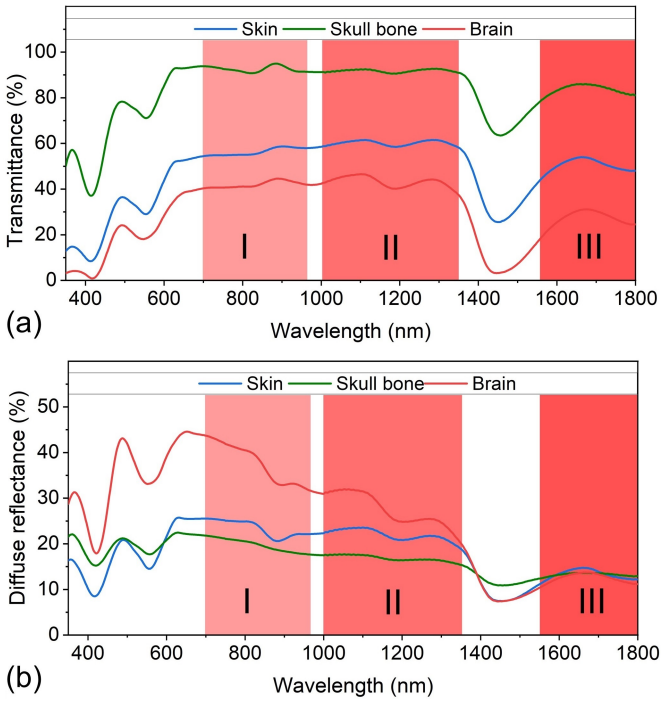


Fig. 4: (a) Total transmittance and (b) diffuse reflectance spectra of mouse head tissues measured with UV/Vis/NIR spectrophotometer. The thicknesses of mouse skin, skull bone, and brain are 0.5 mm, 0.5 mm, and 1 mm, respectively. Three tissue transparency windows were identified: (I) ∼700–950 nm, (II) ∼1000–1350 nm, (III) ∼1550–1870 nm.

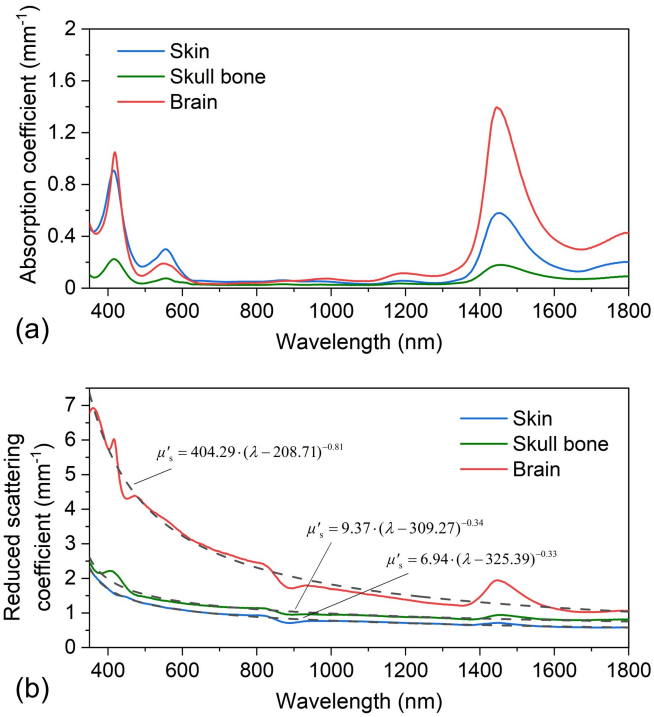


Fig. 5: (a) The absorption coefficient and (b) the reduced scattering coefficient of the freshly harvested mouse brain cortex, skull bone, and head skin. In (b), approximations of the experimental data using the presented formulas are shown.

shown in Fig. 6.

Fig. 6 clearly represents that, depending on the wavelength of the probing radiation, the depth of its penetration into brain tissue varies significantly. The maximum effect is observed in the spectral regions ∼700–900 nm and ∼1050–1150 nm, where the radiation penetrates to a depth of about 2 mm. It is important to note that these spectral regions correspond to the wavelengths of the experimental system considered in this work.

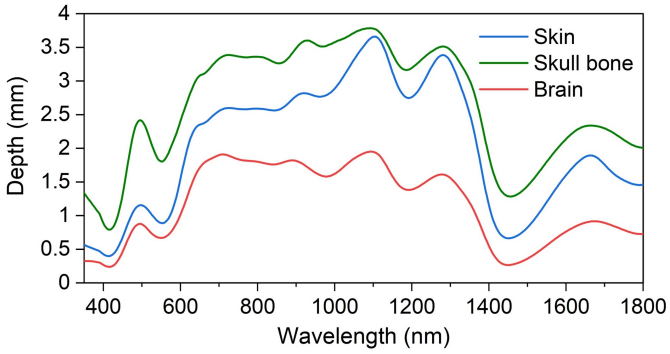


Fig. 6: The depth of light penetration into the mouse head tissue.

### *B. Transmission measurements with CW and pulsed lasers*

We further investigated *ex vivo* mouse samples using CW and pulsed lasers operating in the second biological window and compared the results with transmittance in the first NIR region. Since phytochromes can be activated by absorbing low-intensity light in the far-red and NIR regions [29], [56], we have used a femtosecond pulsed laser in the wavelength range of 750–830 nm that is covered by the first tissue transparency window [57]. This wavelength region is important for the photoconversion of the phytochrome to the inactive state by linear absorption [6], [10], [29]. The investigation of the second biological window is attractive for bioimaging [58]–[60] and two-photon absorption of opsins and phytochromes [29], [61], [62]. Transmittance measurements in the second transparency window were performed using CW and pulsed lasers operating in the wavelength range of 1086–1183 nm. To make a comparison, the parameters of incident beams were matched for both types of lasers. Each measurement was carried out in less than 5 seconds. During the experiments, the tissue temperature did not increase by more than 1.5 °C that was controlled by a thermocouple. For each sample of the skin, skull, and brain, transmittance measurements were repeated three times in different parts of the tissue. Fig. 7 shows the average transmittance values depending on the wavelength of the laser. The results of measurements using a CW laser are presented as a solid line, while the transmittance of mouse head tissues irradiated with a pulsed laser is depicted by a dotted line.

Based on the experimental results, the transmittance of the skin irradiated with the pulsed laser increases by 7% in the wavelength range of 750–830 nm. In the 1086–1183 nm

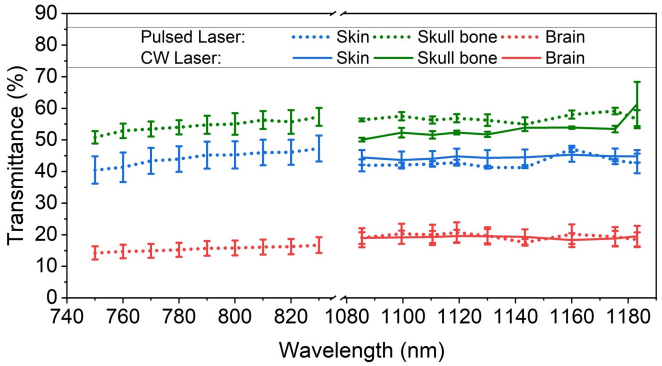


Fig. 7: Transmittance of freshly prepared one-layer mouse head tissues (0.5 mm skin, 0.5 mm skull, and 1 mm brain) irradiated with CW and pulsed lasers at the same point.

region, the value is slightly lower than in the first tissue transparency window (43% at 1086 nm and 47% at 830 nm) due to the gradual increase in light absorption by water [63]. The transmittance spectra of the skull bone and brain cortex are coloured green and red, respectively. In the case of pulsed laser irradiation, both curves demonstrate the growth of light transmittance with increasing wavelength. The reason is a lower absorption of haemoglobin at wavelengths of ∼1000–1350 nm [57]. This leads to less light absorption by oxygenated and deoxygenated blood. Since the proportion of red blood cells in the vessels of skull bone and brain cortex changed significantly after 8 hours [64], the optical properties of the samples were measured no later than one hour after sample preparation. Due to the higher concentration of blood cells in the brain than in the skull, haemoglobin absorption has a more significant effect on brain transmittance spectra. The transmittance of skull bone is about 56%, while the transmittance of 1 mm brain slice is 20%.

Measurements of average power passed through biological tissues irradiated with CW (solid line) and pulsed (dotted line) lasers show that the transmitted power is slightly higher for pulsed irradiation than for CW irradiation in the 2nd wavelength range. The effect is noticeable for the skull bone measurements. For a pulsed laser, the transmittance values vary from 55% to 59%, which is 5 units higher than for a CW laser. For brain tissues, the difference is only up to 1.5 units between pulsed and CW irradiation. Measurements for the skin in experiments with a CW laser have a fairly high uncertainty. This error bar overlaps the values of transmitted power of the pulsed laser and does not give an exact answer whether the tissue transmission value is higher under irradiation with USP. In general, note that the small difference in the measurements in the two laser modes can be explained by the relatively small transfer length in thin samples and the presence of a small number of scattering events.

However, other studies [38], [43] also prove that ultra-short pulses penetrate deeper into biological tissues than a single long pulse of specific energy. In biological tissue, a high photon density of USP laser excites a significant portion of the electrons, which leads to a state close to saturation. That allows the rest of the incoming photons transfer through a temporary transparent irradiated zone. In addition, a decrease in the pulse duration leads to less interaction of the pulse with the tissue and a greater decrease in the absorption and scattering coefficients [43].

For this work, the initial intensity of Gaussian pulses is more than 4 orders of magnitude higher than the intensity of the CW laser. Therefore, even with the same average power, the USP laser can deliver the same energy deeper into a biological sample without overheating it [40], [41].

Since the head tissues have different layers with complicated curvatures that influence the photon migration [65], we additionally measured the transmittance of freshly prepared three- and two-layer mouse head tissues with the use of the pulsed laser (Fig. 8). Three-layer samples included skin, skull bone, and brain and had a thickness of 2.5 mm, while 1 mm thick two-layer head tissues consisted of skin and skull. The thickness of each layer (skin: 0.5 mm; skull: 0.5 mm; brain: 1.5 mm) was measured only after the optical experiments and gentle separation of the layers.

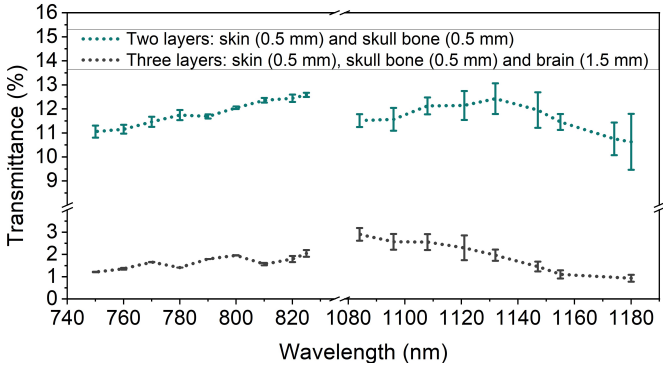


Fig. 8: Transmittance of freshly prepared two-layer and three-layer mouse head tissues irradiated with pulsed laser in 1st and 2nd range.

The experimental results demonstrate that the transmittance of three-layer tissues changes from 1% to 3%. It should be mentioned that the sample included a 1.5 mm brain which is characterised by high light absorption. However, the main optogenetic applications do not require a deep penetration into brain tissues, since the neurons involved in stimulation and monitoring are located in the brain cortex [66]–[68]. Therefore, the main aspect is the light transmittance through the skin and skull bone. The transmittance through two-layer tissues varies from 10% to 13%. In the 1st region, the increase in transmittance is characterised by a decrease in light absorption by blood hemoglobin. In the 2nd region, multilayer samples have a downtrend. It can be explained by a slight increase in light absorption by water [55]. A comparison of the transmission spectra of one-, two- and three-layer head tissues shows that in real in vivo conditions, the light transmission will be further affected by the complicated curvature of the layers, different refractive indices and a higher content of chromophores (in particular, hemoglobin and water).

The USP lasers operating in the second NIR region proved to be efficient in delivering high power to the brain cortex through the skin and skull bone without damage. Since

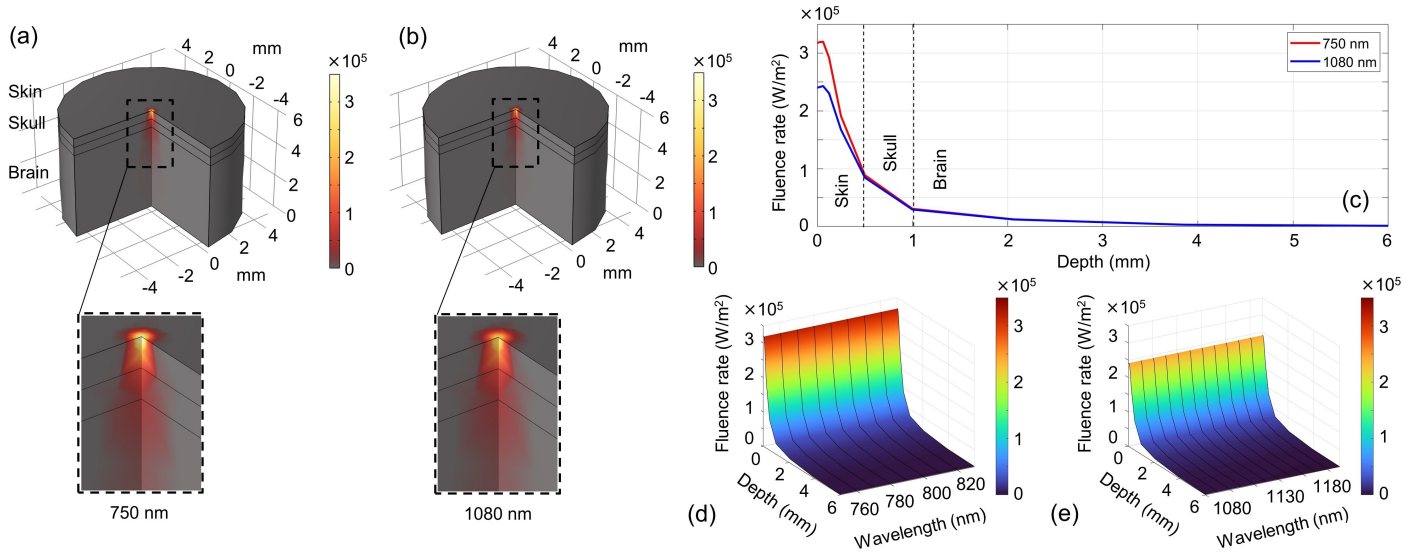


Fig. 9: Fluence rate distribution in the mouse head model for (a) 750 nm and (b) 1080 nm; (c) corresponding quantitative depth-wise fluence rate distribution along the mouse head tissue; quantitative depth-wise fluence rate distribution depending on the wavelength: (d) 1st range, (e) 2nd range.

1190 nm lasers can nonlinearly activate phytochromes [29] and opsins [8], [30], USP lasers operating at this wavelength can reach a penetration depth with required power that will be sufficient for non-linear absorption of opsins/phytochromes in the brain of living animals.

### C. Fluence rate distribution

In this section, the simulated results of effects of laser wavelength on the fluence rate distributions in biological tissue are discussed. Fig. 9a,b show the fluence rate distribution in the mouse head volume. Fig. 9c demonstrates the dependence of the fluence rate on depth. Fig. 9d,e summarise the depth-wise fluence rate distribution for different wavelengths.

These results are consistent with the experimental data collected using the spectrophotometer and our laser system and demonstrate a sufficiently strong attenuation of radiation by the skin and skull bone. Absorption and scattering of the skin reduce the fluence rate by 72% and 65% for the first and second wavelength ranges considered, respectively. The skull bones for both ranges reduce the fluence rate by 65%. Thus, approximately 10% and 12% of the initial radiation in the 1st and 2nd wavelength ranges reach the brain tissues, respectively. At the same time, at 2.5 mm depth (the brain thickness of 1.5 mm), the radiation is significantly attenuated, and only 1-3% of the initial power pass through the complex three-layer mouse head model. These results are in agreement with the experimental data (Fig. 8) that demonstrates the accuracy of the modeling method.

## IV. Conclusions

Since optogenetics applying research advances rapidly, the non-invasive activation of opsins and phytochromes become essential for progress in studying brain normality and pathology. The current light-targeting systems used in optogenetics are limited to hundreds of microns [69]. However, the penetration depth of millimetre range is required for non-invasive neuronal stimulation.

The increase of the penetration depth and the delivery of sufficient power to the brain cortex is possible by changing two main aspects that we reviewed in the paper. The first one is the shift to the second near-infrared transparency window. This is achievable by two-photon activation of opsins [8], [27], [30] and phytochromes [29] at a wavelength range of 1.1–1.3 $\mu$m instead of single-photon excitation at 0.5–0.8 $\mu$m. We demonstrated that the light penetrates into the mouse skin, skull, and brain tissues deeper in the II-NIR transparency window than in visible and I-NIR ranges. The second necessary approach for neuronal stimulation is the use of USP light systems instead of CW or microsecond pulsed illumination sources that are mostly used for optogenetic research [69]–[72]. The first advantage of USP lasers is that ultra-short pulses penetrate deeper into biological tissues than long pulses [43]. Our study proved that for the skull and brain tissues, the light transmittance of II-NIR USP laser is higher than CW laser. The second benefit is a less thermal effect on biological tissues, which has been studied in detail in [22], [40]. The third most import aspect of using the USP lasers in optogenetic tools is the delivery of sufficient power through biological tissues to activate light-sensitive proteins. In this paper, we demonstrated a prototype of a laser system applicable to optogenetic research and studied the efficiency of radiation transport in mouse head tissues. Experimental and simulation results showed that the USP radiation of the developed tunable laser source passes through the mouse head tissues efficiently. More than 10% of the initial radiation passed through the skin and skull samples. Since neurons involved in optogenetic stimulation are located in the brain cortex [66]–[68], this amount of irradiation should be sufficient for the actuation of phytochrome/opsins by two-photon absorption in the area of

light-biotissue interaction. It is worth noting that an additional increase in the depth of penetration can be achieved using optical clearing methods [73], [74], but this is beyond the scope of research in this paper.

The results suggest the possibility of *in vivo* optogenetics in living animals and can be used for further research for non-invasive applications in the photobiomodulation of brain cells.

## REFERENCES


[1] K. Deisseroth, G. Feng, A. K. Majewska, G. Miesenböck, A. Ting, and M. J. Schnitzer, "Next-generation optical technologies for illuminating genetically targeted brain circuits," *J. Neurosci.*, vol. 26, no. 41, pp. 10 380–10 386, 2006.

[2] P. Mahmoudi, H. Veladi, and F. Ghaderi Pakdel, "Optogenetics, tools and applications in neurobiology," *J. Med. Signals Sens.*, vol. 7, pp. 71–79, 04 2017.

[3] B. Rost, F. Schneider-Warme, D. Schmitz, and P. Hegemann, "Optogenetic tools for subcellular applications in neuroscience," *Neuron*, vol. 96, pp. 572–603, 11 2017.

[4] A. Adamantidis, F. Zhang, L. de Lecea, and K. Deisseroth, "Optogenetics: Opsins and optical interfaces in neuroscience," *Cold Spring Harb. Protoc.*, vol. 2014, pp. 815–822, 2014.

[5] A. Björling, O. Berntsson, H. Lehtivuori, H. Takala, A. J. Hughes, M. Panman, M. Hoernke, S. Niebling, L. Henry, R. Henning, I. Kosheleva, V. Chukharev, N. V. Tkachenko, A. Menzel, G. Newby, D. Khakhulin, M. Wulff, J. A. Ihalainen, and S. Westenhoff, "Structural photoactivation of a full-length bacterial phytochrome," *Sci. Adv.*, vol. 2, no. 8, p. e1600920, 2016.

[6] N. C. Rockwell and J. C. Lagarias, "Phytochrome diversification in cyanobacteria and eukaryotic algae," *Curr. Opin. Plant Biol.*, vol. 37, pp. 87–93, 2017.

[7] A. Terakita and T. Nagata, "Functional Properties of Opsins and their Contribution to Light-Sensing Physiology," *Zool. Sci.*, vol. 31, no. 10, pp. 653–659, 2014.

[8] M. K. Engqvist, R. S. McIsaac, P. Dollinger, N. C. Flytzanis, M. Abrams, S. Schor, and F. H. Arnold, "Directed evolution of gloeobacter violaceus rhodopsin spectral properties," *J. Mol. Biol.*, vol. 427, no. 1, pp. 205–220, 2015.

[9] E. A. Ferenczi, X. Tan, and C. L.-H. Huang, "Principles of optogenetic methods and their application to cardiac experimental systems," *Front. Physiol.*, vol. 10, 2019.

[10] V. Lychagov, A. Shemetov, R. Jimenez, and V. Verkhusha, "Microfluidic system for in-flow reversible photoswitching of near-infrared fluorescent proteins," *Anal. Chem.*, vol. 88, p. 11821–11829, 2016.

[11] A. Ulijasz, G. Cornilescu, C. Cornilescu, J. Zhang, M. Rivera, J. Markley, and R. Vierstra, "Structural basis for the photoconversion of a phytochrome to the activated Pfr form," *Nature*, vol. 463, p. 250, 2010.

[12] M. J. Duarte, V. V. Kanumuri, L. D. Landegger, O. Tarabichi, S. Sinha, X. Meng, A. E. Hight, E. D. Kozin, K. M. Stankovic, M. C. Brown, and D. J. Lee, "Ancestral adeno-associated virus vector delivery of opsins to spiral ganglion neurons: Implications for optogenetic cochlear implants," *Mol. Ther.*, vol. 26, no. 8, pp. 1931–1939, 2018.

[13] R. T. Richardson, A. C. Thompson, A. K. Wise, E. A. Ajay, N. Gunewardene, S. J. O'Leary, P. R. Stoddart, and J. B. Fallon, "Viral-mediated transduction of auditory neurons with opsins for optical and hybrid activation," *Sci. Rep.*, vol. 11, no. 1, p. 11229, 2021.

[14] L. Lazzerini Ospri, G. Prusky, and S. Hattar, "Mood, the circadian system, and melanopsin retinal ganglion cells," *Annu. Rev. Neurosci.*, vol. 40, pp. 539–556, 2017.

[15] B. T. Chen, H. J. Yau, C. Hatch, I. Kusumoto-Yoshida, S. L. Cho, F. W. Hopf, and A. Bonci, "Rescuing cocaine-induced prefrontal cortex hypoactivity prevents compulsive cocaine seeking," *Nature*, vol. 496, no. 7445, pp. 359–62, 2013.

[16] A. de Oliveira, A. Reimer, and A. Widge, "T34. effects of repeated cortico-striatal optogenetic stimulation on ocd-like behaviors in rats," *Biol. Psychiatry*, vol. 85, no. 10, p. S142, 2019.

[17] M. H. Berry, A. Holt, A. Salari, J. Veit, M. Visel, J. Levitz, K. Aghi, B. M. Gaub, B. Sivyer, J. G. Flannery, and E. Y. Isacoff, "Restoration of high-sensitivity and adapting vision with a cone opsin," *Nat. Commun.*, vol. 10, no. 1, p. 1221, 2019.

[18] C. Yu, I. R. Cassar, J. Sambangi, and W. M. Grill, "Frequency-specific optogenetic deep brain stimulation of subthalamic nucleus improves parkinsonian motor behaviors," *J. Neurosci.*, vol. 40, p. 4323, 2020.

[19] A. Ingles-Prieto, N. Furthmann, S. H. Crossman, A.-M. Tichy, N. Hoyer, M. Petersen, V. Zheden, J. Biebl, E. Reichhart, A. Gyoergy, D. E. Siekhaus, P. Soba, K. F. Winklhofer, and H. Janovjak, "Optogenetic delivery of trophic signals in a genetic model of parkinson's disease," *PLoS Genet.*, vol. 17, no. 4, p. e1009479, 2021.

[20] Y. Shen, R. E. Campbell, D. C. Côté, and M. E. Paquet, "Challenges for therapeutic applications of opsin-based optogenetic tools in humans," *Front. Neural. Circuits*, vol. 14, p. 41, 2020.

[21] A. Sabeeh and V. Tuchin, "Recent advances in the laser radiation transport through the head tissues of humans and animals – a review," *J. of Biomedical Photonics & Eng.*, vol. 6, no. 4, 2020.

[22] V. Dremin, I. Novikova, and E. Rafailov, "Simulation of thermal field distribution in biological tissue and cell culture media irradiated with infrared wavelengths," *Opt. Express*, vol. 30, no. 13, p. 23078, 2022.

[23] L. Shi, L. A. Sordillo, A. Rodríguez-Contreras, and R. Alfano, "Transmission in near-infrared optical windows for deep brain imaging," *J. Biophotonics*, vol. 9, no. 1-2, pp. 38–43, 2016.

[24] L. A. Sordillo, Y. Pu, S. Pratavieira, Y. Budansky, and R. R. Alfano, "Deep optical imaging of tissue using the second and third near-infrared spectral windows," *J. Biomed. Opt.*, vol. 19, no. 5, p. 056004, 2014.

[25] S. Golovynskyi, I. Golovynska, L. I. Stepanova, O. I. Datsenko, L. Liu, J. Qu, and T. Y. Ohulchanskyy, "Optical windows for head tissues in near-infrared and short-wave infrared regions: Approaching transcranial light applications," *J. Biophotonics*, vol. 11, p. e201800141, 2018.

[26] R. Prakash, O. Yizhar, B. Grewe, C. Ramakrishnan, N. Wang, I. Goshen, A. Packer, D. Peterka, R. Yuste, M. Schnitzer, and K. Deisseroth, "Two-photon optogenetic toolbox for fast inhibition, excitation and bistable modulation," *Nat. Methods*, vol. 9, pp. 1171–1179, 11 2012.

[27] T. Fu, I. Arnoux, J. Döring, H. Backhaus, H. Watari, I. Stasevicius, W. Fan, and A. Stroh, "Exploring two-photon optogenetics beyond 1100 nm for specific and effective all-optical physiology," *iScience*, vol. 24, no. 3, p. 102184, 2021.

[28] I. W. Chen, E. Ronzitti, B. R. Lee, T. L. Daigle, D. Dalkara, H. Zeng, V. Emiliani, and E. Papagiakoumou, "*In vivo* submillisecond two-photon optogenetics with temporally focused patterned light," *J. Neurosci*, vol. 39, no. 18, p. 3484, 2019.

[29] S. G. Sokolovski, E. A. Zherebtsov, R. K. Kar, D. Golonka, R. Stabel, N. B. Chichkov, A. Gorodetsky, I. Schapiro, A. Möglich, and E. U. Rafailov, "Two-photon conversion of a bacterial phytochrome," *Biophys. J.*, vol. 120, no. 5, pp. 964–974, 2021.

[30] M. Hasegawa, T. Hosaka, K. Kojima, Y. Nishimura, Y. Nakajima, T. Kimura-Someya, M. Shirouzu, Y. Sudo, and S. Yoshizawa, "A unique clade of light-driven proton-pumping rhodopsins evolved in the cyanobacterial lineage," *Sci. Rep.*, vol. 10, p. 16752, 10 2020.

[31] M. Mesradi, A. Genoux, V. Cuplov, D. Abi-Haidar, S. Jan, I. Buvat, and F. Pain, "Experimental and analytical comparative study of optical coefficient of fresh and frozen rat tissues," *J. Biomed. Opt.*, vol. 18, no. 11, p. 117010, 2013.

[32] E. A. Genina, A. N. Bashkatov, D. K. Tuchina, P. A. D. (Timoshina), N. Navolokin, A. Shirokov, A. Khorovodov, A. Terskov, M. Klimova, A. Mamedova, I. Blokhina, I. Agranovich, E. Zinchenko, O. V. Semyachkina-Glushkovskaya, and V. V. Tuchin, "Optical properties of brain tissues at the different stages of glioma development in rats: pilot study," *Biomed. Opt. Express*, vol. 10, no. 10, pp. 5182–5197, 2019.

[33] C. P. Sabino, A. M. Deana, T. M. Yoshimura, D. F. da Silva, C. M. França, M. R. Hamblin, and M. S. Ribeiro, "The optical properties of mouse skin in the visible and near infrared spectral regions," *J. Photochem. Photobiol. B: Biol.*, vol. 160, pp. 72–78, 2016.

[34] M. S. Ozturk, M. G. Montero, L. Wang, L. M. Chaible, M. Jechlinger, and R. Prevedel, "Intravital mesoscopic fluorescence molecular tomography allows non-invasive *in vivo* monitoring and quantification of breast cancer growth dynamics," *Commun. Biol.*, vol. 4, p. 556, 2021.

[35] H. Soleimanzad, H. Gurden, and F. Pain, "Optical properties of mice skull bone in the 455- to 705-nm range," *J. Biomed. Opt.*, vol. 22, no. 1, p. 10503, 2017.

[36] J. T. Hashmi, Y.-Y. Huang, S. K. Sharma, D. B. Kurup, L. De Taboada, J. D. Carroll, and M. R. Hamblin, "Effect of pulsing in low-level light therapy," *Lasers Surg. Med.*, vol. 42, no. 6, pp. 450–466, 2010.

[37] D. M. Zezell and P. A. Ana, *High power lasers and their interaction with biological tissues*. John Wiley & Sons, 2015, vol. 33, p. 11.

[38] A. Barbora, O. Bohar, A. A. Sivan, E. Magory, A. Nause, and R. Minnes, "Higher pulse frequency of near-infrared laser irradiation increases penetration depth for novel biomedical applications," *PLOS ONE*, vol. 16, no. 1, p. e0245350, 2021.

[39] D. Han, J. Xu, Z. Wang, N. Yang, X. Li, Y. Qian, G. Li, R. Dai, and S. Xu, "Penetrating effect of high-intensity infrared laser pulses through body tissue," *RSC Adv.*, vol. 8, pp. 32 344–32 357, 2018.

[40] S. Ilic, S. Leichliter, J. Streeter, A. Oron, L. De Taboada, and U. Oron, "Effects of power densities, continuous and pulse frequencies, and number of sessions of low-level laser therapy on intact rat brain," *Photomed. Laser Surg.*, vol. 24, pp. 458–66, 2006.

[41] J. Joensen, K. Øvsthus, R. K. Reed, S. Hummelsund, V. V. Iversen, R. A. B. a. Lopes-Martins, and J. M. Bjordal, "Skin penetration time-profiles for continuous 810 nm and superpulsed 904 nm lasers in a rat model," *Photomed. Laser Surg.*, vol. 30, no. 12, pp. 688–694, 2012.

[42] T. Ando, W. Xuan, T. Xu, T. Dai, S. Sharma, G. Kharkwal, Y.-Y. Huang, Q. Wu, M. Whalen, S. Sato, M. Obara, and M. Hamblin, "Comparison of therapeutic effects between pulsed and continuous wave 810-nm wavelength laser irradiation for traumatic brain injury in mice," *PLOS ONE*, vol. 6, p. e26212, 10 2011.

[43] B. Shariati, S. S. Khatami, M. A. Ansari, F. Jahangiri, H. Latifi, and V. V. Tuchin, "Method for tissue clearing: temporal tissue optical clearing," *Biomed. Opt. Express*, vol. 13, no. 8, pp. 4222–4235, 2022.

[44] X. Song, A. Teng, H. Chen, J. Wei, and L. Song, "Finite element simulation of the interaction between pulsed laser and mouse brain," 02 2021, p. 87.

[45] M. A. Ansari and R. Massudi, "Study of short-pulse laser propagation in biological tissue by means of the boundary element method," *Lasers Med. Sci.*, vol. 26, pp. 503–508, 07 2011.

[46] D. Manahan-Vaughan, "Special considerations when using mice for *in vivo* electrophysiology and long-term studies of hippocampal synaptic plasticity during behavior," in *Handbook of in vivo Neural Plasticity Techniques*. Elsevier, 2018, vol. 28, pp. 63–84.

[47] S. A. Prahl, M. J. C. van Gemert, and A. J. Welch, "Determining the optical properties of turbid media by using the adding–doubling method," *Appl. Opt.*, vol. 32, no. 4, pp. 559–568, 1993.

[48] A. N. Bashkatov, E. A. Genina, and V. V. Tuchin, "Optical properties of skin, subcutaneous, and muscle tissues: A review," *J. Innov. Opt. Health Sci.*, vol. 04, no. 01, pp. 9–38, 2011.

[49] I. E. Rafailov, V. V. Dremin, K. S. Litvinova, A. V. Dunaev, S. G. Sokolovski, and E. U. Rafailov, "Computational model of bladder tissue based on its measured optical properties," *J. Biomed. Opt.*, vol. 21, no. 2, p. 025006, 2016.

[50] T. M. Gonçalves, I. S. Martins, H. F. Silva, V. V. Tuchin, and L. M. Oliveira, "Spectral optical properties of rabbit brain cortex between 200 and 1000 nm," *Photochem.*, vol. 1, no. 2, pp. 190–208, 2021.

[51] B. D. Bunday, *Basic Optimisation Methods*. Edward Arnold, 1984.

[52] A. Ishimaru, *Wave Propagation and Scattering in Random Media*. Elsevier, 1978.

[53] N. Ottosen and H. Petersson, *Introduction to the Finite Element Method*. Prentice-Hall, 1992.

[54] S. R. Arridge, "Optical tomography in medical imaging," *Inverse Probl.*, vol. 15, no. 2, pp. R41–R93, 1999.

[55] G. M. Hale and M. R. Querry, "Optical constants of water in the 200-nm to 200-$\mu$m wavelength region," *Appl. Opt.*, vol. 12, no. 3, pp. 555–563, 1973.

[56] A. V. Leopold and V. V. Verkhusha, "Light control of rtk activity: from technology development to translational research," *Chem. Sci.*, vol. 11, no. 37, pp. 10 019–10 034, 2020.

[57] E. Hemmer, A. Benayas, F. Légaré, and F. Vetrone, "Exploiting the biological windows: current perspectives on fluorescent bioprobes emitting above 1000 nm," *Nanoscale Horiz.*, vol. 1, no. 3, pp. 168–184, 2016.

[58] G. Molodij, A. Sdobnov, Y. Kuznetsov, A. Harmelin, I. Meglinski, and V. Kalchenko, "Time-space Fourier $\kappa\omega'$ filter for motion artifacts compensation during transcranial fluorescence brain imaging," *Phys. Med. Biol.*, vol. 65, no. 7, p. 075007, 2020.

[59] V. Kalchenko, A. Sdobnov, I. Meglinski, Y. Kuznetsov, G. Molodij, and A. Harmelin, "A robust method for adjustment of laser speckle contrast imaging during transcranial mouse brain visualization," *Photonics*, vol. 6, no. 3, 2019.

[60] G. Piavchenko, I. Kozlov, V. Dremin, D. Stavtsev, E. Seryogina, K. Kandurova, V. Shupletsov, K. Lapin, A. Alekseyev, S. Kuznetsov, A. Bykov, A. Dunaev, and I. Meglinski, "Impairments of cerebral blood flow microcirculation in rats brought on by cardiac cessation and respiratory arrest," *J. Biophotonics*, vol. 14, no. 12, p. e202100216, 2021.

[61] A. Guru, R. J. Post, Y.-Y. Ho, and M. R. Warden, "Making sense of optogenetics," *Int. J. Neuropsychopharmacol.*, vol. 18, no. 11, p. pyv079, 2015.

[62] D. Oron, E. Papagiakoumou, F. Anselmi, and V. Emiliani, *Chapter 7 - Two-photon optogenetics*. Elsevier, 2012, vol. 196, pp. 119–143.

[63] L. Sordillo, S. Pratavieira, Y. Pu, K. Salas-Ramirez, L. Shi, L. Zhang, and Y. Budansky, "Third therapeutic spectral window for deep tissue imaging," *Proc. SPIE*, vol. 8940, p. 89400V, 2014.

[64] D.-W. Wu, Y.-M. Li, and F. Wang, "How long can we store blood samples: A systematic review and meta-analysis," *EBioMedicine*, vol. 24, pp. 277–285, 2017.

[65] Y. Liu, S. L. Jacques, M. Azimipour, J. D. Rogers, R. Pashaie, and K. W. Eliceiri, "OptogenSIM: a 3D Monte Carlo simulation platform for light delivery design in optogenetics," *Biomed. Opt. Express*, vol. 6, no. 12, pp. 4859–4870, 2015.

[66] S. Conde-Berriozabal, L. García-Gilabert, E. García-García, L. Sitjà-Roqueta, J. López-Gil, E. Muñoz-Moreno, M. B. Boudjadja, G. Soria, M. J. Rodríguez, J. Alberch, and M. Masana, "Altered m2 cortex - superior colliculus visual perception circuit in huntington's disease," *bioRxiv*, 2022. [Online]. Available: https://www.biorxiv.org/content/early/2022/03/28/2022.03.24.485610

[67] M. Zhang and F. Frohlich, "Cell type-specific excitability probed by optogenetic stimulation depends on the phase of the alpha oscillation," *Brain Stimul.*, vol. 15, no. 2, pp. 472–482, 2022.

[68] Z. Sun, A. Schneider, M. Alyahyay, G. Karvat, and I. Diester, "Effects of optogenetic stimulation of primary somatosensory cortex and its projections to striatum on vibrotactile perception in freely moving rats," *eNeuro*, vol. 8, no. 2, 2021.

[69] E. Ronzitti, C. Ventalon, M. Canepari, B. C. Forget, E. Papagiakoumou, and V. Emiliani, "Recent advances in patterned photostimulation for optogenetics," *J. Opt.*, vol. 19, p. 113001, 2017.

[70] B. V. Zemelman, G. A. Lee, M. Ng, and G. Miesenböck, "Selective photostimulation of genetically charged neurons," *Neuron*, vol. 33, no. 1, pp. 15–22, 2002.

[71] E. Papagiakoumou, F. Anselmi, A. Bègue, V. Sars, J. Glückstad, E. Isacoff, and V. Emiliani, "Scanless two-photon excitation of channelrhodopsin-2," *Nat. Methods*, vol. 7, pp. 848–54, 10 2010.

[72] I.-W. Chen, E. Papagiakoumou, and V. Emiliani, "Towards circuit optogenetics," *Curr. Opin. Neurobiol.*, vol. 50, pp. 179–189, 2018.

[73] D. Zhu, K. V. Larin, Q. Luo, and V. V. Tuchin, "Recent progress in tissue optical clearing," *Laser Photonics Rev.*, vol. 7, no. 5, pp. 732–757, 2013.

[74] A. Sdobnov, M. Darvin, E. Genina, A. Bashkatov, J. Lademann, and V. Tuchin, "Recent progress in tissue optical clearing for spectroscopic application," *Spectrochim. Acta A Mol. Biomol. Spectrosc.*, vol. 197, pp. 216–229, 2018.

**Diana Galiakhmetova** received the BSc degree with first-class honours in physics from Kazan Federal University, Russia, in 2018. There, she gained experience in Mössbauer spectroscopy and received four advanced academic scholarships for scientific achievements. In 2020, she received her MSc degree with the thesis "The stability of single-walled carbon nanotubes saturable absorber for a fiber laser" in The Skolkovo Institute of Science and Technology, Moscow, Russia. As a part of her master degree program, she had research internships in TirPhotonics LLC, Moscow, Russia and Aston Institute of Photonic Technologies, Aston University, Birmingham, UK, where she conducted her research and development of ultra-short pulsed fiber lasers and fiber amplifiers. She is currently pursuing the Ph.D. degree in photonics at Aston Institute of Photonic Technologies, Aston University, Birmingham, UK. Her research interests include the development of ultra-short pulsed lasers and amplifiers for biomedical applications, the study of medical diagnostic and treatment techniques using optogenetic tools, and the fabrication of fiber lasers with the use of carbon nanomaterials as saturable absorbers. Ms. Galiakhmetova's awards and honors include a grant of the Russian Science Foundation, Skoltech President's Scholarship (Skolkovo Institute of Science and Technology, Moscow, Russia, 2020), EAS Postgraduate Research Studentships (Aston University, Birmingham, United Kingdom, 2020), the Return to Research Grant in Optoelectronics 2022, Rank Prize.

**Dr. Viktor Dremin** received his MSc and PhD degrees from Orel State University, Orel, Russia, in 2013 and 2017, respectively. During the first several years of his career, he was involved in the development of new scientific devices for optical remote sensing of the Earth and terrestrial planets as an optoelectronics design engineer of the company "Astron Electronics" (Russia). As a PhD student, Dr. Dremin also conducted active research in biomedical engineering and biophotonics at the R&D Center of Biomedical Photonics (Orel State University, Russia). Part of the PhD research was carried out at Aston University (UK) by Erasmus+ programme. After PhD viva (2017), his work on the development of an imaging system for skin chromophores visualisation at the University of Oulu (Finland) has been supported by EDUFI Fellowship. In 2019, his project to develop a multimodal hyperspectral system for the diagnosis of glycation of biological tissues received the support of a prestigious postdoctoral grant by Marie Skłodowska-Curie Individual Fellowships programme to perform research at Aston University (2020-2022). Currently, he is a Research Fellow at Aston University. His research interests include biomedical imaging, optical tools for assessment of metabolic activity of biological tissues, modelling of optical radiation propagation in biological tissues, etc. He has various prestigious national and international awards. He has authored and co-authored over 100 articles in refereed journals and conference proceedings, 8 patents, and 4 book chapters. His h-index 19; i10-index 34.

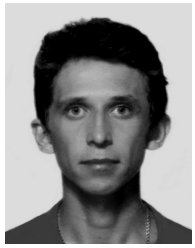

**Dr. Aleksandr Koviarov** is an early-stage postdoc at Aston University. He had been working in an R&D company "Lasers and Optical Systems" Co. Ltd for 7 years. During his job in that company, Dr. Koviarov was engaged in the development of laser with 946 nm wavelength for plasma diagnostic in the ITER's diverter (ITER – The International Thermonuclear Experimental Reactor, megaproject located in Cadarache, France) and high power 532 nm picoseconds laser for the lunar laser ranging. He became an expert in solid-state laser systems, regenerative amplifiers and nonlinear optics and has acquired a strong theoretical background. At the end of 2020, Dr. Koviarov decided to entered academia to begin a research career in Aston University. His current research interests include the development of imaging methods for cancer diagnostics, fiber laser systems, nonlinear optics, and ultrafast lasers. He has over 10 publications in refereed journals and conference proceedings.

**Dr. Dmitrii Stoliarov** received his PhD degree from Ulyanovsk State University, Ulyanovsk, Russia, in 2019. In 2020, he joined the Optoelectronics and Biomedical Photonics Group, Aston University, Birmingham, UK. As a highly skilled specialist with a strong track record in Optics, Laser Physics, Nonlinear, and Fiber Optics he has been involved in a numerous international research projects. The latest research interests include optical frequency combs, high-repetition-rate mode-locked lasers and nonlinear frequency conversion. Research outcomes of Dr. Stoliarov were published in more than 50 publications in high-impact journals and conference proceedings.

**Dr. Neville Ngum** is a Postdoctoral Research Associate with expertise in single cell and network electrophysiology. He obtained his BSc degree in Medical Laboratory Sciences from the University of Buea, MSc in Molecular Toxicology from Aston University and PhD from the University of Nottingham in 2019 where he investigated the components of the giant Indian centipede for NaV1.7 ion channel modifiers. He then moved to the University of East Anglia as a senior research associate to investigate novel antagonists of P2X4 receptors and probe their bind kinetics and mechanisms of actions. He is currently exploring methods of non-invasive dynamic neural control by laser-based technology for treatments of neurodegenerative diseases at Aston University.

**Dr. Raghavan Chinnambedu Murugesan** received the PhD in Materials Science-Crystals Growth from Crystal Growth Centre, Anna University, India, in 2009. From 2009 to 2017 worked as post-doc/Research Professor at various Universities, Sungkyunkwan University (2009-2011), Changwon National University (2011-2016), South Korea, National Taiwan University, Taiwan (2017-2018). Later, he moved to the UK as Marie Curie Research Fellow (2018-2020) at AIPT, Aston University, and continued as Research Associate in the ERDF-ETICC project (2020-2022), He is currently a Research Associate in the ERDF-AGRI project, providing technical and scientific solutions for SME's, especially solutions through photonics for the Food & Agri sectors. His research interests include bulk single crystals, functional nanomaterials, and thin films for electronic, optoelectronic, and photonic applications. His awards and honors include the Marie S. Curie Individual fellowship, European Union, Brain Korea 21 (BK21) fellowship, South Korea, and Senior Research Fellowship (SRF), Council of Scientific & Industrial Research (CSIR), India.

**Prof. Rheinallt Parri** was born in Deiniolen, Wales. He received his BSc in Physiology and Pharmacology in 1988 and PhD in Neurophysiology in 1992 from Southampton University, UK. He completed Postdoctoral research at the University of California, San Francisco and at Cardiff University before being appointed as a lecturer at Aston University in 2004, and Professor in 2021. He is a neuroscientist using primarily cell electrophysiological and optical techniques with research interests in the interactions between glia and neurons that control network excitability, and mechanisms underlying synaptic and network plasticity. Rheinallt Parri has editorial roles for Frontiers in Cellular Neuroscience, Cells and Brain Sciences.

**Dr. Sergei Sokolovski** was born in Minsk, Belarus, USSR in 1963. He received his BSc and MSc degrees with Distinction in Biology/Biochemistry from Belorussian State University in 1989 and PhD degree in Biophysics/Photobiology from Belorussian Natl Academy of Sciences in 1993. Since then he was working in Senior Research positions in Jena, Karlsruhe (Germany), York, Glasgow, Dundee, and Aston Birmingham (UK) Universities in the inter-disciplinary field of plant photobiology, regulation of cell membrane traffic, and plasma membrane ion channel activities, biophotonics, medical spectroscopy diagnostics. He has over 3 years of experience in cell membrane biophysics, photobiomodulation cellular oxidative stress, laser cancer, and vascular system diagnostics and therapy. Academia and industrial collaborating work both national and international have resulted in over 70 peer-reviewed and conference proceeding publications (nearly 2000 citations, h-index 21) author and co-investigator of 9 successful grant applications gained from UK and EU Commission funding bodies.

**Prof. Edik U. Rafailov** (Senior Member, IEEE) received the Ph.D. degree from Ioffe Institute, Saint Petersburg, Russia, in 1992. In 1997, he moved to St. Andrews University, Scotland, UK and in 2005, he established a new group in Dundee University, Scotland, UK. In 2014, he and his Optoelectronics and Biomedical Photonics Group moved to Aston University, Birmingham, UK. He has authored and coauthored more than 500 articles in refereed journals and conference proceedings, including three books, ten invited chapters and numerous plenary/invited talks. His current research interests include high-power CW and ultra-short pulsed lasers, generation of UV/visible/IR/MIR and THz radiation, nanostructures, nonlinear and integrated optics, and biomedical photonics. He coordinated the €14.7M FP7 FAST-DOT project development of new ultrafast lasers for biophotonics applications and the €12.5M NEWLED project which aims to develop a new generation of white LEDs. He also coordinated the H2020 FET projects: Mesa-Brain (€3.3M, aims to develop 3D nano-printing technology for functional three-dimensional human stem cell derived neural networks), NEUROPA (€3.6M, aims to develop novel non-invasive theragnostic approaches), and PLATFORMA. He also leads a few other projects funded by EU FP7, H2020 and EPSRC.